

## Acoustic scattering from functionally graded cylindrical shells

J. JAMALI, M. H. NAEI, F. HONARVAR, M. RAJABI

*Department of Mechanical Engineering  
University of Tehran  
Amirabad, Teheran, Iran  
e-mail: jjamaly@ut.ac.ir*

IN THIS PAPER, the method of wave function expansion is adopted to study the scattering of a plane harmonic acoustic wave incident upon an arbitrarily thick-walled, functionally graded cylindrical shell submerged in and filled with compressible ideal fluids. A laminate approximate model and the so-called state space formulation in conjunction with the classical transfer matrix (T-matrix) approach, are employed to present an analytical solution based on the three-dimensional exact equations of elasticity. Three models, representing the elastic properties of FGM interlayer are considered. In all models, the mechanical properties of the graded shell are assumed to vary smoothly and continuously with the change of volume concentrations of the constituting materials across the thickness of the shell. In the first two models, the rule of mixture governs. The main difference between them is the set of elastic constants (e.g., Lamé's constants in model I and Young's modulus and Poisson's ratio in Model II) which are governed by the rule of mixtures. In the third model, an elegant self-consistent micromechanical model which assumes an interconnected skeletal microstructure in the graded region is employed. Particular attention is paid to back-scattered acoustic response of these models in a wide range of frequency and for different shell wall-thicknesses. The results reveal a technical comparison between these models. In addition, by examining various cases (i.e., different shell wall-thicknesses, various profiles of variations and different volume concentration of constituents), the impact of the overall volume concentration of constituents and also the profile of variations, on the resonant response of the graded shell is investigated. Limiting cases are considered and good agreement with the solutions available in the literature is obtained.

**Key words:** resonance acoustic spectroscopy, FGM cylindrical shell, state-space method, surface waves.

Copyright © 2011 by IPPT PAN

### 1. Introduction

IN RECENT YEARS, the study of functionally graded materials (FGMs) has attracted a lot of attention. FGMs are a new generation of composite materials characterized by a continuously varying property due to a continuous change in the microstructural gradients (e.g., composition, morphology and crystal structure) across their thickness [1, 2]. It takes advantage of certain desirable features of each constituent phases and optimizes the distribution of material properties

such as strength, hardness, thermal resistance, etc., so that the desired responses to given mechanical and thermal loadings are achieved [3–5].

The scattered pressure field from the target contains valuable information about the characteristics of the target and the surrounding medium. Appropriate exploitation of this information and proper identification of the resonance frequencies of the elastic object can serve as a powerful tool in many applications such as material characterization and non-destructive testing/evaluation of materials [6, 7], remote classification of submerged targets [8, 9] and on-line monitoring of elastic components [10]. The comprehensive reviews of the sound scattering problems from cylindrical components and extensive bibliographies can be found in the works of GAUNAURD [11], ÜBERALL [12], and VEKSLER [13]; here we just point out some of the most related work in this area.

KADUCHAK and LOEFFLER [14] analyzed the backscattering effects due to filling of the interior cavity of a submerged cylindrical shell with a higher impedance fluid such as water. VEKSLER and IZBICKI [15] proposed a procedure for modal resonance isolation in the scattering problems of a plane acoustic wave by cylindrical and spherical shells. HONARVAR and SINCLAIR [16] developed an exact normal-mode expansion for scattering of a compression acoustic wave from an immersed, transversely isotropic solid cylinder. They allowed the incident acoustic wave to make an arbitrary angle with the normal to the cylindrical surface, and examined the effect of elastic constant changes on resonance frequencies of an isotropic aluminum cylinder. JOO *et al.* [17] subsequently extended the concept of the inherent background to multilayered elastic cylindrical structures by solving the problem of acoustic wave scattering, by an analogous liquid structure. CONOIR *et al.* [18] studied the resonances of an air-filled elastic cylindrical shell immersed in a fluid using the phase gradient method, which is based on the phase derivative of the scattering matrix with regard to the frequency. CHOI *et al.* [19, 20] considered resonance scattering of acoustic waves from submerged penetrable targets of canonical geometry (e.g., an empty cylindrical or spherical elastic shell in a fluid) and proposed exact expressions, named the inherent background coefficients, which is obtained from the zero-frequency limit of an equivalent fluid target, in order to properly describe the acoustical background over the entire frequency range. JOO *et al.* [21] subsequently extended the concept of the inherent background to multilayered elastic cylindrical structures by solving the problem of acoustic wave scattering, by an analogous liquid structure. ÜBERALL [22] reviewed the physical phenomena that arise in the scattering of acoustic waves from fluid-immersed elastic (metallic, spherical and cylindrical) shells, which may be either evacuated or filled with the same or with a different fluid. He discussed the various phenomena occurring, including the formation of circumferential (peripheral or “surface”) waves that circumnavigate the shells, propagating either as elastic waves in the shell material or as fluid-borne waves of the Scholte–Stoneley-type in the external or the internal fluid. KIM and IH [23] used

the normal mode expansion technique to present a resonance scattering analysis for oblique incidence of a plane acoustic wave upon an air-filled, transversely isotropic cylindrical shell immersed in water. FAN *et al.* [24] studied the circumferential resonance modes of an immersed solid elastic cylinder which is insonified by an obliquely incident plane acoustic wave over a large range of incidence angles. They employed the Resonance Scattering Theory to derive physical explanations for singular features of their frequency-incidence angle plots. HASHEMINEJAD and RAJABI [25] extended the HONARVAR and SINCLAIR'S [16] analytical solution (for oblique incidence of a plane acoustic wave upon a water-submerged, transversely isotropic solid cylinder) to that of a fully orthotropic cylindrical shell of arbitrary thickness, based on the three-dimensional exact equations of anisotropic elasticity. They used their solutions to correlate the perturbation in the material elastic constants of an aluminium cylindrical shell to the sensitivity of resonances associated with various modes of wave propagation, appearing in the backscattered amplitude spectrum (i.e., axially guided, Lamb, Rayleigh and Whispering Gallery waves). Most recently, HASHEMINEJAD and RAJABI [26] employed an exact treatment based on the inherent background coefficients to investigate the resonance scattering of time-harmonic plane acoustic waves by functionally graded cylindrical shells, at normal incidence. In this work, they just focused on the modal response of the graded shell and their primary goal was to exhibit the capability of the inherent background theories in order to isolate the modal resonance response of the structure.

The resonances are the fingerprints of specimens. For NDE and on-line monitoring purposes, these resonances are used to evaluate various properties of cylindrical structures by matching the measured data to theoretical models through iterative algorithms (e.g., the measured form function amplitude in resonance acoustic spectroscopy technique). Therefore, the precision of the process is strictly dependent on the accuracy of the theoretical model. In literature, many models exist which describe the elasticity of graded shells. The compatibility between the theoretical models and the measured response depend on many factors such as the manufacturing condition, operating state, etc; but it is important to identify the frequency-dependent deviation which may occur due to the incorrect recognition of the proper model. In this work, we employ a laminate approximate model along with the so-called state space formulation in conjunction with the transfer matrix (T-matrix) approach, to interrogate the back-scattered acoustic response of three practical elastic models of FGMs in a wide frequency range. Also, by the aid of the classic resonance scattering theorem, the behavior of the resonance frequencies of the graded shells to the variation of the overall volume fraction of constituting materials for different profiles of distribution is investigated. This work would serve as an extension of the existing analytical solution for normal incidence of a plane acoustic wave upon a water-submerged, isotropic, functionally graded cylindrical shell [26] to that of a fully orthotropic, functionally graded cylindrical shell. In the

extended formulation, the incident waves can insonify the cylindrical shell at any desired angle. We show that how the resonance frequencies of the graded cylindrical components can be utilized as an indicator of the overall volume fractions and the profile of distribution of their constituents. The results reveal a number of technical points for the resonance acoustic spectroscopy purposes of cylindrical component with graded material properties.

## 2. Formulation

### 2.1. Basic acoustic field equations

Figure 1 shows an infinite plane acoustic wave of frequency  $\omega/2\pi$  incident at an angle  $\alpha$  on a submerged and fluid-filled orthotropic-FGM cylindrical shell of infinite length, inner radius  $a_0$  and outer radius  $a_q$ .  $(x, y, z)$  is the Cartesian coordinate system with origin at  $O$  and  $z$  direction, coincident with the axis

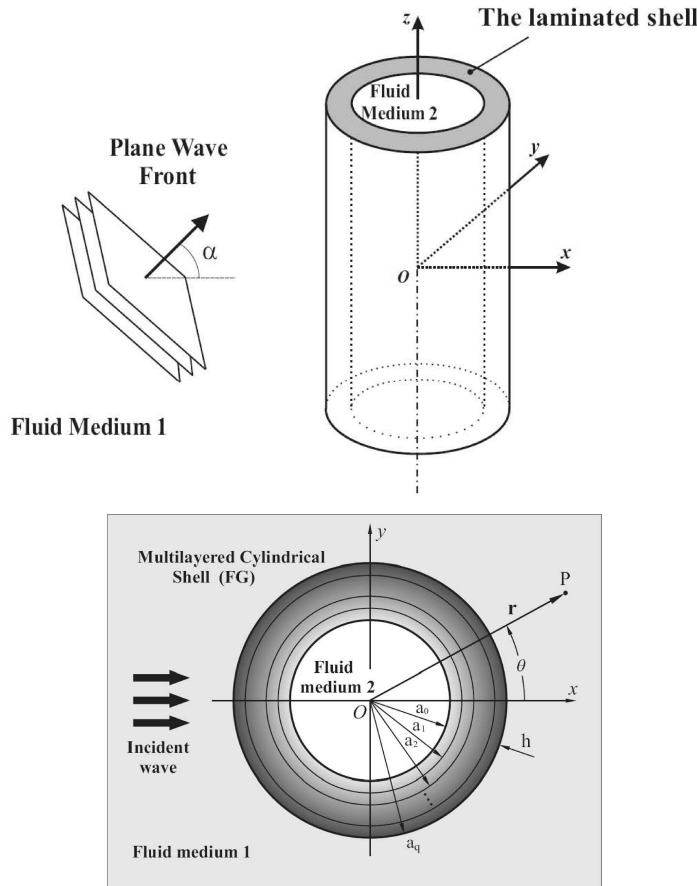


FIG. 1. Problem geometry.

of the cylindrical shell, and  $(r, \theta, z)$  is the corresponding cylindrical coordinate system. The field equations for an inviscid and ideal compressible medium that can not support shear stresses, may conveniently be expressed in terms of a scalar velocity potential  $\varphi$  as [27],

$$(2.1) \quad \mathbf{v} = -\nabla\varphi, \quad p = -i\omega\rho\varphi, \quad \nabla^2\varphi + K^2\varphi = 0,$$

where  $K = \omega/c$  is the wave number for the dilatational wave,  $c$  is the speed of sound,  $\rho$  is the ambient density,  $\mathbf{v}$  is the fluid particle velocity vector, and  $p$  is the acoustic pressure. The expansion of the incident plane wave, propagating in the surrounding fluid medium, in a cylindrical coordinate system (see Fig. 1) has the form [27],

$$(2.2) \quad \varphi_{\text{inc}}(r, \theta, \omega) = \varphi_0 \sum_{n=0}^{\infty} \varepsilon_n i^n J_n(K_{1,r}r) \cos(n\theta) e^{i(k_z z - \omega t)},$$

where  $k_z = K_1 \sin \alpha$ ,  $K_{1,r} = K_1 \cos \alpha$  and  $K_1 = \omega/c_1$  is the wave number in the outer fluid medium 1 (see Fig. 1),  $J_n$  is the cylindrical Bessel function of the first kind of order  $n$ .  $\varepsilon_n$  is the Neumann factor ( $\varepsilon_n = 1$  for  $n = 0$ , and  $\varepsilon_n = 2$  for  $n > 0$ ),  $i = \sqrt{-1}$ , and  $\varphi_0$  is the amplitude of the incident wave. Likewise, the scattered potential in the surrounding fluid medium 1, and the transmitted potential in the inner fluid medium 2, can be expressed as a linear combination of cylindrical waves as [27],

$$(2.3) \quad \begin{aligned} \varphi_1(r, \theta, \omega) &= \sum_{n=0}^{\infty} \varepsilon_n i^n A_n(\omega) H_n^{(1)}(K_{1,r}r) \cos(n\theta) e^{i(k_z z - \omega t)}, \\ \varphi_2(r, \theta, \omega) &= \sum_{n=0}^{\infty} \varepsilon_n i^n B_n(\omega) J_n(K_{2,r}r) \cos(n\theta) e^{i(k_z z - \omega t)}, \end{aligned}$$

where  $K_{2,r} = \sqrt{K_2^2 - k_z^2}$ , and  $K_2 = \omega/c_2$  is the acoustic wave number in the inner medium 2,  $H_n^{(1)}(x) = J_n(x) + iY_n(x)$  is the cylindrical Hankel function of the first kind of order  $n$ ,  $Y_n(x)$  is the cylindrical Bessel function of the second kind of order  $n$ , and  $A_n$  and  $B_n$  are unknown scattering and transmission coefficients. Furthermore, using Eq. (2.1), the acoustic pressures and radial velocities in the fluid media 1 and 2 are respectively written as

$$(2.4) \quad \begin{aligned} p_1 &= -i\omega\rho_1(\varphi_{\text{inc}} + \varphi_1) \\ &= -\omega\rho_1 \sum_{n=0}^{\infty} i^{n+1} \varepsilon_n \left[ \varphi_0 J_n(K_{1,r}r) + H_n^{(1)}(K_{1,r}r) A_n(\omega) \right] \cos(n\theta) e^{i(k_z z - \omega t)}, \\ p_2 &= -i\omega\rho_2\varphi_2 = -\sum_{n=0}^{\infty} \omega\rho_2 \varepsilon_n i^{n+1} J_n(K_{2,r}r) B_n(\omega) \cos(n\theta) e^{i(k_z z - \omega t)}, \end{aligned}$$

and

$$\begin{aligned}
 v_r^{(1)} &= -\frac{\partial(\varphi_{\text{inc}} + \varphi_1)}{\partial r} \\
 (2.5) \quad &= -K_{1,r} \sum_{n=0}^{\infty} \varepsilon_n i^n \left[ \varphi_0 J'_n(K_{1,r}r) + H_n^{(1)'}(K_{1,r}r) A_n(\omega) \right] \cos(n\theta) e^{i(k_z z - \omega t)}, \\
 v_r^{(2)} &= -\frac{\partial \varphi_2}{\partial r} = -K_{2,r} \sum_{n=0}^{\infty} \varepsilon_n i^n J'_n(K_{2,r}r) B_n(\omega) \cos(n\theta) e^{i(k_z z - \omega t)},
 \end{aligned}$$

where prime denotes differentiation with respect to the argument.

## 2.2. Sandwich cylindrical shell

Now, we consider a sandwich cylindrical shell of uniform thickness  $h$ , with a functionally graded interlayer core of uniform thickness  $h_I$ , inner radius  $a_0$  and outer radius  $a_q$ , with variable material properties suspended in and filled with ideal compressible fluids. Adopting a laminate model [26, 28, 29], the sandwich cylindrical shell is assumed to be composed of  $q$  sublayers of homogeneous orthotropic materials, which are perfectly bonded at their interfaces and lined up such that their axes of symmetry coincide with each other (Fig. 1). The solution is expected to gradually approach the exact one as the number of sublayers increases. The material properties within each layer of inner radius  $a_{k-1}$ , outer radius  $a_k$  and uniform thickness  $h_k = a_k - a_{k-1}$ , are described by the elastic coefficients  $c_{ij}^k$  and mass density  $\rho_c^k$  where  $k = 1, \dots, q$ . In what follows, we look for a technique to solve the equations of motion for the  $k$ -th layer of the multilayered cylindrical shell.

**2.2.1. Local transfer matrix.** Let us consider a hollow cylinder of infinite length with orthotropic sublayers. For the  $k$ -th layer, the equations of motion, in absence of body forces and in terms of stress components, are written as [30]

$$\begin{aligned}
 (2.6) \quad &\frac{\partial \sigma_{rr}^k}{\partial r} + \frac{\partial \sigma_{r\theta}^k}{r \partial \theta} + \frac{\partial \sigma_{rz}^k}{\partial z} + \frac{1}{r} (\sigma_{rr}^k - \sigma_{\theta\theta}^k) = \rho_c^k \frac{\partial^2 u_r^k}{\partial t^2}, \\
 &\frac{\partial \sigma_{r\theta}^k}{\partial r} + \frac{\partial \sigma_{\theta\theta}^k}{r \partial \theta} + \frac{\partial \sigma_{z\theta}^k}{\partial z} + \frac{2}{r} \sigma_{r\theta}^k = \rho_c^k \frac{\partial^2 u_\theta^k}{\partial t^2}, \\
 &\frac{\partial \sigma_{rz}^k}{\partial r} + \frac{\partial \sigma_{\theta z}^k}{r \partial \theta} + \frac{\partial \sigma_{zz}^k}{\partial z} + \frac{\sigma_{rz}^k}{r} = \rho_c^k \frac{\partial^2 u_z^k}{\partial t^2},
 \end{aligned}$$

where  $\rho_c^k$  is the solid material density, and  $u_r^k$ ,  $u_\theta^k$  and  $u_z^k$  are the material displacements in the  $r$ ,  $\theta$  and  $z$  directions, respectively. Moreover, noting that a cylindrically orthotropic homogeneous material is characterized by nine independent

elastic constants, the generalized Hooke's law in a cylindrical coordinate system for the  $k$ -th layer may be written as [31]:

$$(2.7) \quad \begin{pmatrix} \sigma_{rr}^k \\ \sigma_{\theta\theta}^k \\ \sigma_{zz}^k \\ \sigma_{\theta z}^k \\ \sigma_{rz}^k \\ \sigma_{r\theta}^k \end{pmatrix} = \begin{bmatrix} c_{11}^k & c_{12}^k & c_{13}^k & 0 & 0 & 0 \\ c_{12}^k & c_{22}^k & c_{23}^k & 0 & 0 & 0 \\ c_{13}^k & c_{23}^k & c_{33}^k & 0 & 0 & 0 \\ 0 & 0 & 0 & c_{44}^k & 0 & 0 \\ 0 & 0 & 0 & 0 & c_{55}^k & 0 \\ 0 & 0 & 0 & 0 & 0 & c_{66}^k \end{bmatrix} \begin{pmatrix} \varepsilon_{rr}^k \\ \varepsilon_{\theta\theta}^k \\ \varepsilon_{zz}^k \\ 2\varepsilon_{\theta z}^k \\ v2\varepsilon_{rz}^k \\ 2\varepsilon_{r\theta}^k \end{pmatrix},$$

where  $c_{ij}^k$  are the elastic constants and  $\varepsilon_{ij}^k$  are the strain components defined as:

$$(2.8) \quad \begin{aligned} \varepsilon_{rr}^k &= \frac{\partial u_r^k}{\partial r}, & \varepsilon_{\theta\theta}^k &= \frac{\partial u_\theta^k}{r\partial\theta} + \frac{u_r^k}{r}, & \varepsilon_{zz}^k &= \frac{\partial u_z^k}{\partial z}, \\ \varepsilon_{r\theta}^k &= \frac{1}{2} \left( \frac{\partial u_r^k}{r\partial\theta} + \frac{\partial u_\theta^k}{\partial r} - \frac{u_\theta^k}{r} \right), \\ \varepsilon_{\theta z}^k &= \frac{1}{2} \left( \frac{\partial u_z^k}{r\partial\theta} + \frac{\partial u_\theta^k}{\partial z} \right), \\ \varepsilon_{rz}^k &= \frac{1}{2} \left( \frac{\partial u_z^k}{\partial r} + \frac{\partial u_r^k}{\partial z} \right). \end{aligned}$$

Following the state space approach [28, 29], the state equations can be derived by direct substitution of constitutive equation, Eq. (2.7), and kinematic equation, Eq. (2.8), into equations of motion, Eq. (2.6), which after some tedious manipulations lead to:

$$(2.9) \quad \frac{\partial \mathbf{Y}^k}{\partial r} = \mathbf{M}^k \mathbf{Y}^k,$$

where  $\mathbf{Y}^k = [u_z^k, u_\theta^k, u_r^k, \sigma_{rr}^k, \sigma_{r\theta}^k, \sigma_{rz}^k]^T$  is the state vector, and  $\mathbf{M}^k$  is a  $6 \times 6$  coefficient matrix whose elements are given in Appendix I. Next, by employing normal mode expansion, the state vector  $\mathbf{Y}^k$  is expanded in terms of unknown modal coefficients as

$$(2.10) \quad \mathbf{Y}^k = \begin{pmatrix} u_z^k \\ u_\theta^k \\ u_r^k \\ \sigma_{rr}^k \\ \sigma_{r\theta}^k \\ \sigma_{rz}^k \end{pmatrix} = \sum_{n=0}^{\infty} \begin{pmatrix} a_q u_{z,n}^k(\xi) \cos(n\theta) \\ a_q u_{\theta,n}^k(\xi) \sin(n\theta) \\ a_q u_{r,n}^k(\xi) \cos(n\theta) \\ c_{44}^q \sigma_{rr,n}^k(\xi) \cos(n\theta) \\ c_{44}^q \sigma_{r\theta,n}^k(\xi) \sin(n\theta) \\ c_{44}^q \sigma_{rz,n}^k(\xi) \cos(n\theta) \end{pmatrix} e^{i(k_z z - \omega t)},$$

where  $\xi = r/a_q$  is the dimensionless radial coordinate and  $c_{44}^q$  is one of the elements of the stiffness matrix of the  $q$ -th layer (outer layer) of the multilayered shell. Subsequent substitution of Eq. (2.10) into Eq. (2.9) and utilization of the orthogonality of trigonometric functions, gives

$$(2.11) \quad \frac{d\mathbf{V}_n^k}{d\xi} = \mathbf{D}_n^k(\xi)\mathbf{V}_n^k,$$

where  $\mathbf{V}_n^k = [u_{z,n}^k, u_{\theta,n}^k, u_{r,n}^k, \sigma_{rr,n}^k, \sigma_{r\theta,n}^k, \sigma_{rz,n}^k]^T$  is the modal state vector, and  $\mathbf{D}_n^k(\xi)$  is a  $6 \times 6$  modal coefficient matrix whose elements are given in Appendix II. A laminate approximate model is adopted for solving of the equations [28, 29]. As the thickness of each sublayer is supposed to be very small, the coefficient matrix can advantageously be assumed to be constant within each sublayer. This coefficient matrix is denoted as  $\mathbf{D}_n^k(\xi_{k-1})$  for the  $k$ -th sublayer, where  $\xi_{k-1} = a_{k-1}/a_q$ . Thus, within the  $k$ -th sublayer, the solution to Eq. (2.11) can be written as

$$(2.12) \quad \mathbf{V}_n^k(\xi) = \mathbf{V}_n^k(\xi_{k-1}) \exp \left[ (\xi - \xi_{k-1}) \mathbf{D}_n^k(\xi_{k-1}) \right],$$

where  $\xi_{k-1} \leq \xi \leq \xi_k$ , and  $k = 1, \dots, q$ . Subsequent evaluation of Eq. (2.12) at the outer surface of the  $k$ -th sublayer, leads to the following useful recurrence equation:

$$(2.13) \quad \mathbf{V}_n^k(\xi_k) = \mathbf{L}_n^k \mathbf{V}_n^k(\xi_{k-1}),$$

where  $\mathbf{L}_n^k = \exp[h_k \mathbf{D}_n^k(\xi_{k-1})/a_q]$  is a  $6 \times 6$  local transfer matrix corresponding to the  $k$ -th layer of the multilayered cylindrical shell, which relates the state variables at the outer surface of the  $k$ -th sublayer to those at the inner surface.

**2.2.2. Global transfer matrix and boundary conditions.** By invoking the continuity conditions between all interface layers, the state variables at the outer radius of the cylindrical shell (i.e., at  $r = a_q$  for which  $\xi_q = 1$ ) are advantageously related to those at the inner radius (i.e., at  $r = a_0$  for which  $\xi_0 = a_0/a_q$ ) by

$$(2.14) \quad \mathbf{V}_n^q(\xi_q) = \mathbf{T}_n \mathbf{V}_n^1(\xi_0),$$

where  $\mathbf{T}_n = \prod_{k=1}^q \mathbf{L}_n^k = \prod_{k=1}^q \exp[h_k \mathbf{D}_n^k(\xi_{k-1})/a_q]$  is the  $6 \times 6$  global modal transfer matrix.

The unknown coefficients  $A_n$  and  $B_n$  and the elements of the modal state variable vector,  $\mathbf{V}_n^1(\xi_0) = [u_{z,n}^0, u_{\theta,n}^0, u_{r,n}^0, \sigma_{rr,n}^0, \sigma_{r\theta,n}^0, \sigma_{rz,n}^0]^T$ , can be determined from the boundary conditions imposed at the inner ( $r = a_0$ ) and outer ( $r = a_q$ ) surfaces of the multilayered shell. By assuming continuity of normal fluid and

solid velocities, normal stress and fluid pressure and vanishing of tangential stress at boundaries  $r = a_0$  and  $r = a_q$ , we can write:

$$(2.15) \quad \begin{aligned} (-i\omega)u_r(r, \theta, \omega)|_{r=a_0, a_q} &= v_r(r, \theta, \omega)|_{r=a_0, a_q}, \\ \sigma_{rr}(r, \theta, \omega)|_{r=a_0, a_q} &= -p(r, \theta, \omega)|_{r=a_0, a_q}, \\ \sigma_{r\theta}(r, \theta, \omega)|_{r=a_0, a_q} &= \sigma_{rz}(r, \theta, \omega)|_{r=a_0, a_q} = 0. \end{aligned}$$

Now, making use of Eqs. (2.4), (2.5) and Eq. (2.14) in Eq. (2.15), we obtain the following  $8 \times 8$  coupled linear system of equations:

$$(2.16) \quad \begin{bmatrix} C_{1,n} & 0 & T_n^{3,1} & T_n^{3,2} & T_n^{3,3} & T_n^{3,4} & T_n^{3,5} & T_n^{3,6} \\ 0 & C_{2,n} & 0 & 0 & 1 & 0 & 0 & 0 \\ C_{3,n} & 0 & T_n^{4,1} & T_n^{4,2} & T_n^{4,3} & T_n^{4,4} & T_n^{4,5} & T_n^{4,6} \\ 0 & C_{4,n} & 0 & 0 & 0 & 1 & 0 & 0 \\ 0 & 0 & T_n^{5,1} & T_n^{5,2} & T_n^{5,3} & T_n^{5,4} & T_n^{5,5} & T_n^{5,6} \\ 0 & 0 & 0 & 0 & 0 & 0 & 1 & 0 \\ 0 & 0 & T_n^{6,1} & T_n^{6,2} & T_n^{6,3} & T_n^{6,4} & T_n^{6,5} & T_n^{6,6} \\ 0 & 0 & 0 & 0 & 0 & 0 & 0 & 1 \end{bmatrix} \begin{Bmatrix} A_n \\ B_n \\ u_{z,n}^0 \\ u_{\theta,n}^0 \\ u_{r,n}^0 \\ \sigma_{rr,n}^0 \\ \sigma_{r\theta,n}^0 \\ \sigma_{rz,n}^0 \end{Bmatrix} = \begin{bmatrix} C_{5,n} \\ 0 \\ C_{6,n} \\ 0 \\ 0 \\ 0 \\ 0 \\ 0 \end{bmatrix},$$

where  $T_n^{i,j}$  ( $i, j = 1, 2, \dots, 6$ ) are elements of the global modal transfer matrix,  $T_n$ , and

$$(2.17) \quad \begin{aligned} C_{1,n} &= -K_{1,r}\varepsilon_n i^{n-1} H_n^{(1)'}(K_{1,r}a_q)/\omega a_q, \\ C_{2,n} &= -K_{2,r}\varepsilon_n i^{n-1} J_n'(K_{2,r}a_0)/\omega a_q, \\ C_{3,n} &= -\omega\rho_1\varepsilon_n i^{n+1} H_n^{(1)}(K_{1,r}a_q)/c_{44}^q, \\ C_{4,n} &= \omega\rho_2\varepsilon_n i^{n+1} J_n(K_{2,r}a_0)/c_{44}^q, \\ C_{5,n} &= \varphi_0 K_{1,r}\varepsilon_n i^{n-1} J_n'(K_{1,r}a_q)/\omega a_q, \\ C_{6,n} &= \omega\rho_1\varphi_0\varepsilon_n i^{n+1} J_n(K_{1,r}a_q)/c_{44}^q. \end{aligned}$$

### 2.3. Functionally graded model

In the case of orthotropic FGMs, we use the rule of mixtures in order to find the elastic properties as [28],

$$(2.18) \quad \begin{aligned} c_{ij}^k &= V_F(\bar{r}_k) c_{ij}^1 + [1 - V_F(\bar{r}_k)] c_{ij}^q, \\ \rho^k &= V_F(\bar{r}_k)\rho^1 + [1 - V_F(\bar{r}_k)]\rho^q, \end{aligned}$$

where  $\bar{r}_k = (a_{k-1} + a_k)/2$  ( $k = 1, 2, \dots, q$ ) and  $V_F(\bar{r}_k)$  is the volume fraction of the constituting materials in the  $k$ -th sublayer. The given solution is based

on a high degree of anisotropy (i.e. cylindrically orthotropic) for functionally graded constituents, and can easily be reduced to simpler cases (e.g., isotropic cylinders). Since the isotropic materials are more common in practice, our results will be focused on isotropic materials. For this purpose, three practical models for isotropic FGMs are summarized as follows.

**2.3.1. Model I.** The first model is as same as the model used by HASHEMINEJAD and RAJABI [26], in which the rule of mixture governs on the Lamé constants and the material density function of graded shell. Considering the aforementioned laminate model of the cylindrical shell, we have

$$(2.19) \quad \begin{aligned} \lambda^k &= V_F(\bar{r}_k)\lambda^1 + [1 - V_F(\bar{r}_k)]\lambda^q, \\ \mu^k &= V_F(\bar{r}_k)\mu^1 + [1 - V_F(\bar{r}_k)]\mu^q, \\ \rho^k &= V_F(\bar{r}_k)\rho^1 + [1 - V_F(\bar{r}_k)]\rho^q. \end{aligned}$$

Also, the elastic constants of the sublayeres can be expressed in terms of these Lamé constants as

$$(2.20) \quad \begin{aligned} c_{11}^k &= c_{22}^k = c_{33}^k = \lambda^k + 2\mu^k, \\ c_{12}^k &= c_{13}^k = c_{23}^k = \lambda^k, \\ c_{44}^k &= c_{55}^k = c_{66}^k = \mu^k. \end{aligned}$$

**2.3.2. Model II.** In this model, the Young modulus,  $E^k$ , and the Poisson ratio,  $\nu^k$ , of the graded shell are assumed to be the elastic properties governed by the rule of mixtures:

$$(2.21) \quad \begin{aligned} E^k &= V_F(\bar{r}_k)E^1 + [1 - V_F(\bar{r}_k)]E^q, \\ \nu^k &= V_F(\bar{r}_k)\nu^1 + [1 - V_F(\bar{r}_k)]\nu^q, \\ \rho^k &= V_F(\bar{r}_k)\rho^1 + [1 - V_F(\bar{r}_k)]\rho^q. \end{aligned}$$

The elastic constants of sublayeres are expressed as

$$(2.22) \quad \begin{aligned} c_{11}^k &= c_{22}^k = c_{33}^k = \frac{E^k(1 - \nu^k)}{(1 + \nu^k)(1 - 2\nu^k)}, \\ c_{12}^k &= c_{13}^k = c_{23}^k = \frac{E^k\nu^k}{(1 + \nu^k)(1 - 2\nu^k)}, \\ c_{44}^k &= c_{55}^k = c_{66}^k = \frac{E^k}{2(1 + \nu^k)}. \end{aligned}$$

**2.3.3. Model III.** In this model, an elegant self-consistent micromechanical model [32, 33], which assumes an interconnected skeletal microstructure in the graded

region, is employed. According to this model, no distinctions between the constituent phases are made and the same overall moduli are predicted in another composite in which the roles of the phases are interchanged. Consequently, the locally effective bulk modulus of the FGM interlayer may be related to the elastic moduli of the constituent materials as

$$(2.23) \quad K^k = \left[ \frac{1 - V_F^k(\bar{r}_k)}{K^q + 4\mu^k/3} + \frac{V_F^k(\bar{r}_k)}{K^1 + 4\mu^k/3} \right]^{-1} - \frac{4\mu^k}{3}.$$

Also,  $\mu^k$  (effective shear modulus of the  $k$ -th layer) is obtained by solving the following quartic equation:

$$(2.24) \quad \frac{[1 - V_F^k(\bar{r}_k)]K^q}{K^q + 4\mu^k/3} + \frac{V_F^k(\bar{r}_k)K^1}{K^1 + 4\mu^k/3} + 5 \left\{ \frac{[1 - V_F^k(\bar{r}_k)]\mu^1}{\mu^k - \mu^1} + \frac{V_F^k(\bar{r}_k)\mu^q}{\mu^k - \mu^q} \right\} + 2 = 0.$$

Also, assuming that the density ratio contrast between constituents is not too high, it is appropriate to assume that the effective density of the FGM interlayer is the mean density, given by the straightforward rule-of-mixtures as

$$(2.25) \quad \rho^k = V_F(\bar{r}_k)\rho^1 + [1 - V_F(\bar{r}_k)]\rho^q,$$

and the elastic constants of the sublayeres can be expressed as

$$(2.26) \quad \begin{aligned} c_{11}^k &= c_{22}^k = c_{33}^k = K^k + 4\mu^k/3, \\ c_{12}^k &= c_{13}^k = c_{23}^k = K^k - 2\mu^k/3, \\ c_{44}^k &= c_{55}^k = c_{66}^k = \mu^k. \end{aligned}$$

#### 2.4. The global and resonance scattering coefficients

The most relevant field quantities associated with acoustic resonance scattering are the global and resonance scattering coefficients. The global scattering coefficient may be obtained from the standard definition of the backscattering form-function amplitude [34],

$$(2.27) \quad |f_\infty(\theta = \pi, \omega)| \approx \lim_{r \rightarrow \infty} \sqrt{\frac{2r}{a_q}} \left| \frac{\varphi_1(r, \theta = \pi, \omega)}{\varphi_{\text{inc}}} \right| = \left| \sum_{n=0}^{\infty} f_n(\theta = \pi, K_1 a_q) \right|,$$

where

$$(2.28) \quad f_n(\theta, K_1, a_q) = \frac{2\varepsilon_n}{\sqrt{\pi i K_1 a_q}} A_n \cos(n\theta),$$

is referred to as the global scattering coefficient for the  $n$ -th mode. Consequently, the pure resonances in the scattering amplitudes of the  $n$ -th normal mode can be isolated by subtracting the inherent backgrounds from the global form function as follows [34]:

$$(2.29) \quad |f_n^{(\text{res})}(\theta, K_1 a_q)| = |f_n(\theta, K_1 a_q) - f_n^{(b)}(\theta, K_1 a_q)|,$$

where the inherent background coefficients are defined as:

$$(2.30) \quad f_n^{(b)}(\theta, K_1 a_q) = \frac{2\varepsilon_n}{\sqrt{\pi i K_1 a_q}} A_n^{(b)} \cos(n\theta).$$

The background scattering coefficient,  $A_n^{(b)}$ , which is determined by solving the problem of interaction of a plane acoustic wave with an analogous multilayered fluid shell (i.e., by setting the transverse wave speeds in all of the solid layers equal to zero), is defined as [34]

$$(2.31) \quad A_n^{(b)} = (-1) \frac{K_{1,r} a_q J_n'(K_{1,r} a_q) - [G_n(0^+)]_q J_n(K_{1,r} a_q)}{K_{1,r} a_q H_n^{(1)'}(K_{1,r} a_q) - [G_n(0^+)]_q H_n(K_{1,r} a_q)},$$

where the superscript “ $b$ ” denotes the acoustical background and  $[G_n(0^+)]_q$  is the zero limit of the acceleration function, associated with the outer ( $q$ -th) layer of the multilayered shell structure that, for the  $n = 0$  mode, can be obtained through the following recurrence relation [34, 35]:

$$(2.32)_1 \quad \begin{aligned} [G_n(0^+)]_0 &= \frac{4\rho_c^{(2)}}{\rho_2 - 4\rho_c^{(1)} \ln(1 - h_1/a_1)}, \\ [G_n(0^+)]_k &= \frac{\rho_c^{k+1}}{\rho_c^k} \frac{[G_n(0^+)]_{k-1}}{[1 - \ln(1 - h_k/a_k)][G_n(0^+)]_{k-1}}, \\ [G_n(0^+)]_q &= \frac{\rho_1}{\rho_c^q} \frac{[G_n(0^+)]_{q-1}}{[1 - \ln(1 - h_q/a_{q+1})][G_n(0^+)]_{q-1}}, \end{aligned}$$

where  $k = 1, 2, \dots, q-1$ , and similarly for the  $n \geq 1$  modes,

$$(2.32)_2 \quad \begin{aligned} [G_n(0^+)]_0 &= \frac{\rho_c^{(1)}}{\rho_2} n, \\ [G_n(0^+)]_k &= \frac{\rho_c^{k+1}}{\rho_c^k} \frac{n^2 + l_k [G_n(0^+)]_{k+1}}{l_k + [G_n(0^+)]_{k-1}}, \\ [G_n(0^+)]_q &= \frac{\rho_1}{\rho_c^q} \frac{n^2 + l_q [G_n(0^+)]_{q-1}}{l_q + [G_n(0^+)]_{q-1}}, \end{aligned}$$

in which  $l_k = n \frac{1 + (1 - h_k/a_k)^{2n}}{1 - (1 - h_k/a_k)^{2n}}$  and  $k = 1, 2, \dots, q-1$ . This completes the solution required for the exact resonance scattering analysis of an orthotropic functionally graded cylindrical shell in an acoustic medium. Next we consider some numerical examples.

### 3. Numerical results

In order to illustrate the nature and general behavior of the solution, we consider some numerical examples. Realizing the large number of parameters involved here while keeping in view our computing hardware limitations, we confine our attention to a particular problem. The surrounding and filling fluids are respectively assumed to be water ( $\rho_1 = 1000 \text{ kg/m}^3$ ,  $c_1 = 1480 \text{ m/s}$ ) and air ( $\rho_2 = 1.2 \text{ kg/m}^3$ ,  $c_2 = 344 \text{ m/s}$ ) at atmospheric pressure and ambient temperature.

The cylindrical shell is assumed to be three-layered, in which the interlayer (thickness  $h_I = h_{i+1} + h_{i+2} + \dots + h_{j-1} + h_j$ ,  $i > 0$  and  $j < q$ ) is graded in the radial direction with varying proportions of metallic aluminium (Al) substrate

Table 1. Material properties

Material	$\rho_s$ [kg/m <sup>3</sup> ]	$c_{11}, c_{22}, c_{33}$ [GPa]	$c_{44}, c_{55}, c_{66}$ [GPa]	$c_{12}, c_{13}, c_{23}$ [GPa]
Aluminium (Al)	2706	110.47	26.69	57.09
Zirconia (ZrO <sub>2</sub> )	5700	318.60	94.80	129.00

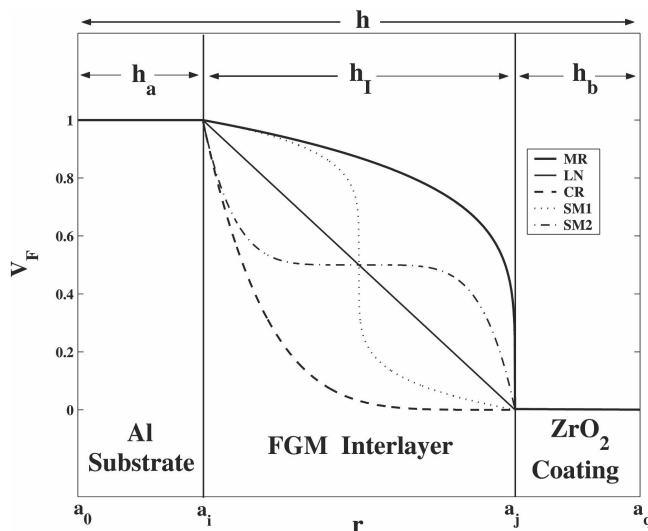


FIG. 2. Variations in volume fraction of aluminum in a general composition of sandwich shell with FGM interlayer.

(thickness  $h_a = h_1 + \dots + h_i$ ) and ceramic zirconia ( $\text{ZrO}_2$ ) coating (thickness  $h_b = h_{j+1} + h_{j+2} + \dots + h_q$ ). The volume fraction of metal in the FGM interlayer is varied from 100% on the inner interface (at  $r = a_0 + h_a = a_i$ ) to zero on the outer interface (at  $r = a_0 + h_a + h_I = a_j$ ). A typical variation in volume fraction of Al along the radial axis is shown in Fig. 2. In this work, two distinct gradient profile families for the functionally graded interphase are studied in this work. In the first family, called power-law distribution, the volume fraction of Al in  $a_i \leq r \leq a_j$  is

$$(3.1)_1 \quad V_F(r) = \left(1 - \frac{r - a_i}{h_I}\right)^\gamma,$$

and for the second family, called sigmoidal distribution, we have

$$(3.1)_2 \quad V_F(r) = \begin{cases} \frac{1}{2} + \frac{1}{2} \left[1 - \frac{2(r - a_i)}{h}\right]^\gamma, & a_i < r < a_i + (h_I/2), \\ \frac{1}{2} - \frac{1}{2} \left[\frac{2(r - a_i)}{h} - 1\right]^\gamma, & a_i + (h_I/2) < r < a_j. \end{cases}$$

Also, the overall volume concentration of Al (inner constituent) may be calculated as written in the following form:

$$(3.2) \quad \bar{V}_F = \frac{\int_{a_0}^{a_q} V_F(r) r dr}{\int_{a_0}^{a_q} r dr}.$$

A MATLAB code was constructed for computing the global transfer matrix,  $\mathbf{T}_n$ , treating boundary conditions and to calculate the unknown scattering coefficients, and the global and the inherent background coefficients as functions of the nondimensional frequency  $K_1 a_q$  for a unit amplitude incident plane wave ( $\varphi_0 = 1$ ). The computations were performed on a Pentium IV personal computer with a maximum number of layers  $q_{\max} = 100$ , a maximum truncation constant of  $n_{\max} = (K_1 a_q)_{\max} + 15$ , especially selected to assure convergence in case of a thick FGM interlayer and also in the high-frequency range. The convergence was systematically checked in a simple trial and error manner, by increasing the number of layers,  $q$ , as well as the truncation constant (i.e., by including more modes in all summations), while looking for steadiness or stability in the numerical value of the solutions.

In the research work made by HASHEMINEJAD and RAJABI [26], the effect of relative thickness of FGM mid-layer (i.e.,  $h_I/h$  on the resonant response of the structure has been studied, where the total thickness of the shell is assumed to be constant (i.e.,  $h/a_q = 0.1$ ). Therefore, here we just focus on the case that the Al substrate and the  $\text{ZrO}_2$  coating are absent (i.e., we have a single-layer functionally graded cylindrical shell;  $h_a = h_b = 0$ ,  $h_I/h = 1$ ).

### 3.1. Comparison of elastic models

Figures 3a through d compare the frequency response of Model I (solid-line), Model II (dotted-line) and Model III (dashed-line), by exhibiting the variations of the backscattering form function amplitude,  $|f(\theta = \pi, K_1 a_q)|$ , with dimensionless frequency,  $K_1 a_q$ , for thin  $h/a_q = 0.04$  thick  $h/a_q = 0.1$  very thick  $h/a_q = 0.25$  and hollow cylinder  $h/a_q = 0.5$ , functionally graded cylindrical shells respectively. A linear distribution of constituting materials according to the power-law variation (i.e.,  $\gamma = 1$  has been considered. As Fig. 3 shows, the dips and peaks (i.e., resonances) associated to the response of Model III have a left-ward shift in comparison to those associated to the Models I and II, especially for higher frequencies and for higher thicknesses. In our frequency range, the maximum relative errors may reach 15 percent which, in the case of improper recognition of the model, may lead to an extraordinary inaccuracy in NDE process. Considering Figures 4a–f which compare the variation of the elastic properties (i.e.,  $E$ ,  $\nu$ ,  $\lambda$ ,  $\mu$ ,  $\kappa$ ) and the mass density (i.e.,  $\rho$ ) along the radial axis (i.e., dimensionless radial coordinate:  $\bar{r} = r/a_q$ , for Models I, II and III, this trend may be interpreted in this way that the Models I and II supply the higher overall stiffness for the graded shell in comparison to the Model III.

As shown in Fig. 3, in a considerably wide range of frequencies (i.e.,  $0 \leq K_1 a_q < 80$  for a thin shell,  $0 \leq K_1 a_q < 60$  for a thick shell,  $0 \leq K_1 a_q < 35$  for a very thick shell and  $0 \leq K_1 a_q < 20$  for a hollow cylinder), the response of the Models I and II are almost identical; but as the frequency increases, the difference between them increases. Initially, these differences demonstrate themselves as slight resonance frequency variations (i.e., peaks and dips), but for higher frequencies, these variations convert to a left-ward frequency shift of Model II in comparison to Model I. Also, in the case of hollow cylinder,  $h/a_q = 0.5$  we observe a completely different response for  $80 \leq K_1 a_q$ . As Figure 4 exhibits, the profile of variation of “Young’s modulus” and “ $\mu$ ” in both models are nearly identical; but the difference in profile of variation of “Poisson’s ratio” and “Lambda” is the main cause of the observed differences in the response of these models.

### 3.2. FGM material inspection

In what follows, we study the effects of the overall volume concentration of constituting materials and the profile of variations on the frequency response of a thick ( $h/a_q = 0.9$ ) and a thin ( $h/a_q = 0.04$ ) graded cylindrical shell, where a power-law distribution governs the variations of elastic properties. Using a root-finder code, the constant  $\gamma$  in Eq. (3.1)<sub>1</sub> is found so that the discrete values corresponding to overall volume concentration of Al is obtained. For the shell with 0.9 thickness, the discrete values of  $\bar{V}_F = [0.0; 0.1; 0.2; \dots; 1.0]$  are obtained as  $\gamma = [+∞; 3.66; 1.95; 1.25; 0.86; 0.61; 0.42; 0.28; 0.16; 0.07; 0.0]$ . For the

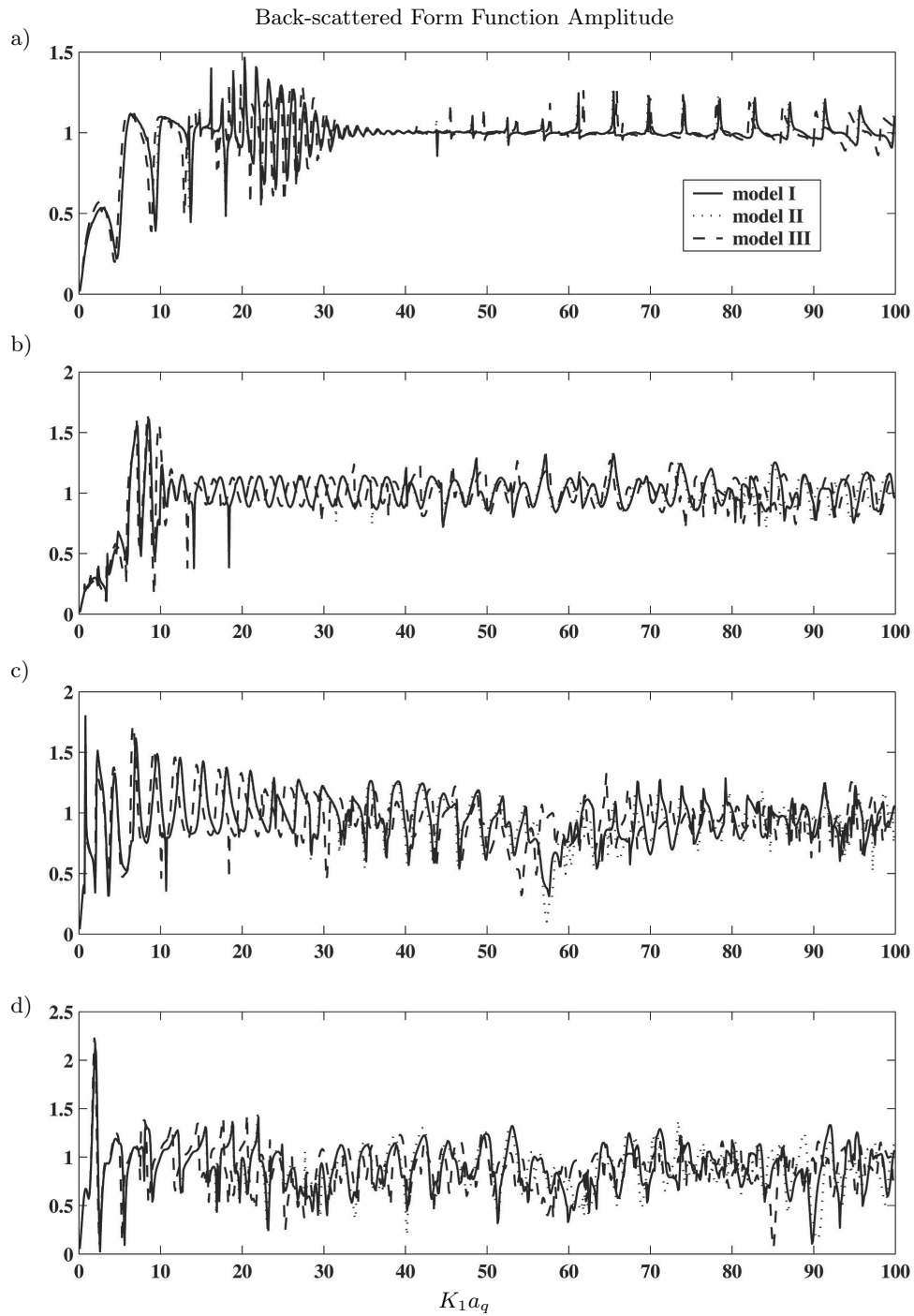


Fig. 3. Variations of backscattering form function amplitudes with selected thicknesses: a)  $h/a_q = 0.04$ , b)  $h/a_q = 0.1$ , c)  $h/a_q = 0.25$ , d)  $h/a_q = 0.5$ , for a functionally graded cylindrical shell with linear profile of variation (i.e.,  $\gamma = 1$ ).

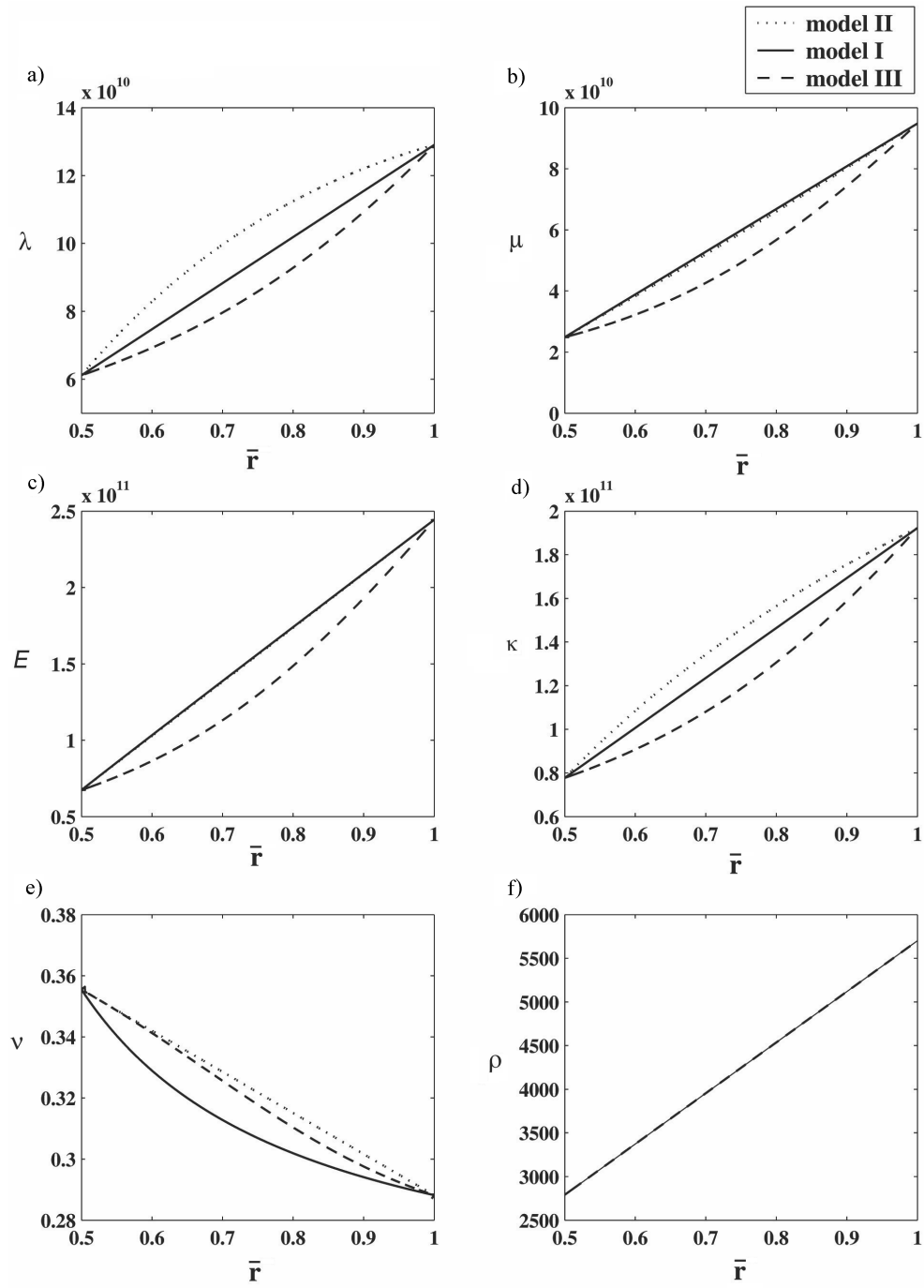


FIG. 4. Variations of elasticity properties with normalized radial coordinate; a)  $\lambda(\bar{r})$ , b)  $\mu(\bar{r})$ , c)  $E(\bar{r})$ , d)  $\kappa(\bar{r})$ , e)  $\nu(\bar{r})$ , f)  $\rho(\bar{r})$  for a thick ( $h/a_q = 0.5$ ), functionally graded hollow cylinder with linear profile of variation (i.e.,  $\gamma = 1$ ).

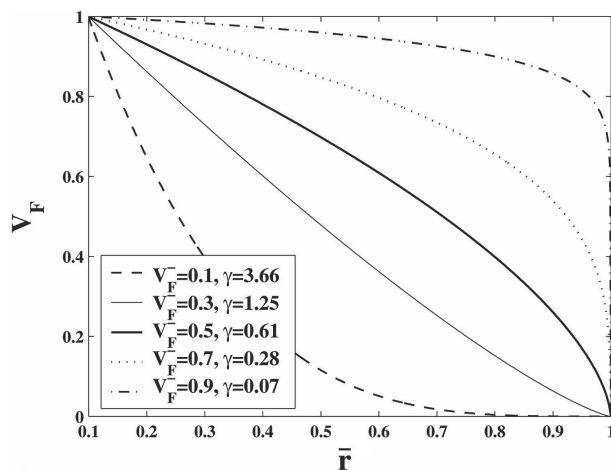


FIG. 5. Variations in volume fraction of aluminum in FGM interlayer of a thick ( $h/a_q = 0.9$ ) functionally graded hollow cylinder in case of power-law distribution.

thin shell with 0.04 thickness for the same values of  $\bar{V}_F = [0.0; 0.1; 0.2; \dots; 1.0]$ , we set  $\gamma = +\infty; 8.93; 4.05; 2.35; 1.5; 1.0; 0.67; 0.43; 0.25; 0.11; 0.0$ . It should be noted that  $\bar{V}_F = 1.0$  corresponds to a single Al shell and,  $\bar{V}_F = 0.0$  corresponds to a single  $\text{ZrO}_2$  shell. While in the theory  $\gamma \rightarrow \infty$  corresponds to a  $\text{ZrO}_2$  shell, it was found that the lower limit of  $\gamma$  for a single  $\text{ZrO}_2$  shell (i.e.,  $\bar{V}_F < 0.01$ ) may be set approximately to  $\gamma \cong 10^2$ . Figure 5 shows the volume fraction profiles for some discrete values of overall volume concentration of Al (i.e.,  $\bar{V}_F = 0.1; 0.3; 0.5; 0.7; 0.9$ ) along the radial axis of the thick shell. To better study the effects of the overall volume concentration of constituting materials and the profile of variations on the frequency response of the graded shell, Figs. 6a–c shows the variations of the modal resonance scattering coefficients,  $|f_n^{(\text{res})}(\theta = \pi, K_1 a_q)|$  [i.e., a)  $n = 0$ , b)  $n = 1$ , c)  $n = 2$ ], for the selected values of volume concentration of constituents. In the case of a thin shell, Fig. 7 shows the volume fraction profiles for some of the discrete values of overall volume concentration of Al (i.e.,  $\bar{V}_F = 0.1; 0.3; 0.5; 0.7; 0.9$ ) along the radial axis. Also Figs. 8a–c show the variations of the modal resonance scattering coefficients,  $|f_n^{(\text{res})}(\theta = \pi, K_1 a_q)|$  (i.e., a)  $n = 2$ , b)  $n = 6$ , (c)  $n = 8$ ), for selected values of volume concentration of constituents. The most important observations are as follows.

It is well-known that the elastic response consists of a smooth background and a resonance spectrum. The resonance modes in the spectrum are linked to the standing surface waves which are formed around the cylindrical shell. The global scattering coefficients perfectly coincide with the inherent background coefficients, except in the resonance region where the resonances are clearly isolated

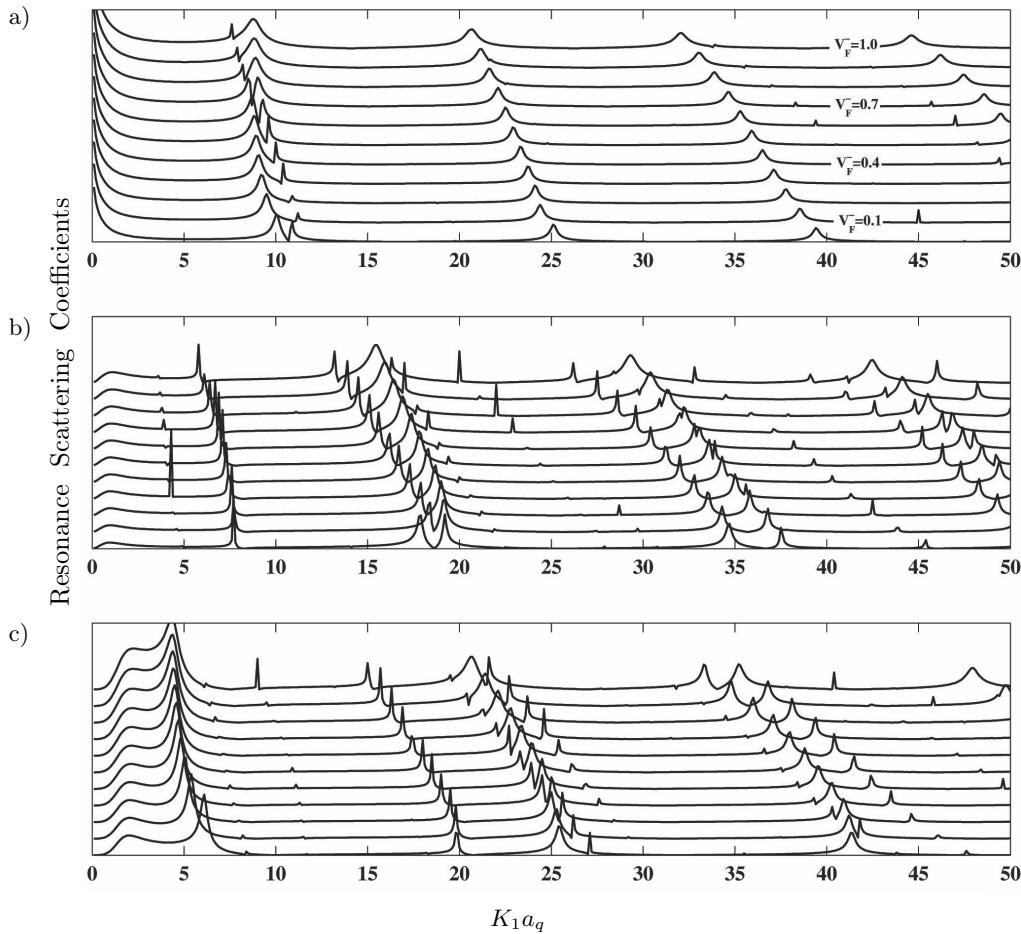


Fig. 6. Variations of the normalized resonance scattering coefficients; a)  $n = 0$ , b)  $n = 1$ , c)  $n = 2$  with dimensionless frequency, for a thick ( $h/a_q = 0.9$ ) functionally graded hollow cylinder, in case of power-law distribution and for selected values of volume fraction concentration of Al.

in Figs. 6 and 8. The dependence of the resonance frequencies on the overall volume concentration of constituting materials and the profile of variations, can be observed more clearly with these resonance spectra in Figs. 6 and 8 than on the backscattering form function amplitudes [26]. The isolated resonances in the case of the thick shell in Fig. 6 are the Rayleigh type or the Whispering Gallery type waves, and the isolated resonances in the case of the thin shell in Fig. 8 are Lamb-type or fluid-born A-type waves. Furthermore, in the  $n = 0$  case (monopole mode) in Fig. 6, a notably high peak which is known in the literature to be associated with the “giant monopole” resonance (i.e., analogous to the situation of air bubbles in water) is observed at a very low frequency [36].

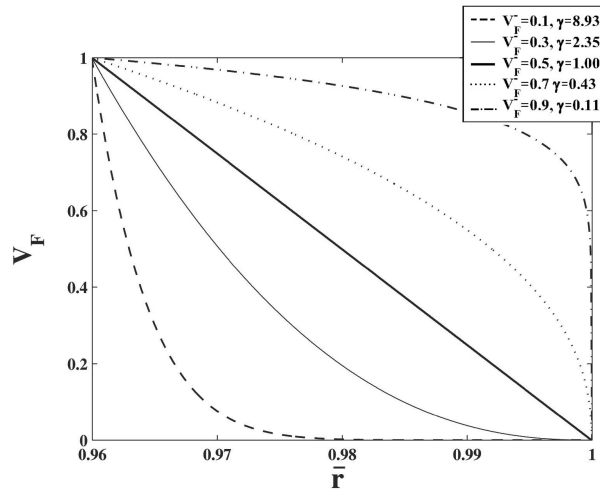


Fig. 7. Variations in volume fraction of aluminum in FGM interlayer of a thin ( $h/a_q = 0.04$ ), functionally graded hollow cylinder in case of power-law distribution.

The resonances of the FGM shell with different overall volume concentrations of constituents and different profiles of variations, for both the thick and thin shells in Figs. 6 and 8 have different characteristics of surface wave propagation and radiation damping. Both the amplitude and the quality of resonances which are visible in these spectra vary with the change in the gradients fraction and the style of distribution. The resonance frequencies of the thick and thin-graded shells are nearly between those of the Al (i.e.,  $\bar{V}_F = 1$ ) and  $\text{ZrO}_2$  (i.e.,  $\bar{V}_F = 0$ ) shells, in the considered range of frequencies: the former is the low frequency bound and the latter is the high frequency bound. As  $\bar{V}_F$  changes from zero to one, the resonances of the graded shell vary from the resonances corresponding to the single  $\text{ZrO}_2$  shell, to the resonances of the single Al shell and a general left-ward shift is observed. In particular, several resonances (especially in the case of a thick shell) are observed that show approximately linear and monotonic behavior with respect to the linear change of overall volume fractions of constituents. This linear correlation may be linked to the fact that these resonances are primarily the function of the overall volume concentration of Al rather than the profile of distribution. Moreover, it can be shown that this monotonic behavior and linear variation of resonances is consistent with the dependence of phase velocities of their corresponding surface waves to the overall volume fraction of constituents. These behaviors show that the frequencies of these dominant resonances alone can be a good indicator of the overall volume fraction of ingredients. However, for evaluating the profile of distribution, a number of resonances must be examined. In addition, when the partial mode number  $n$  increases, the resonance frequencies (especially with higher ex-

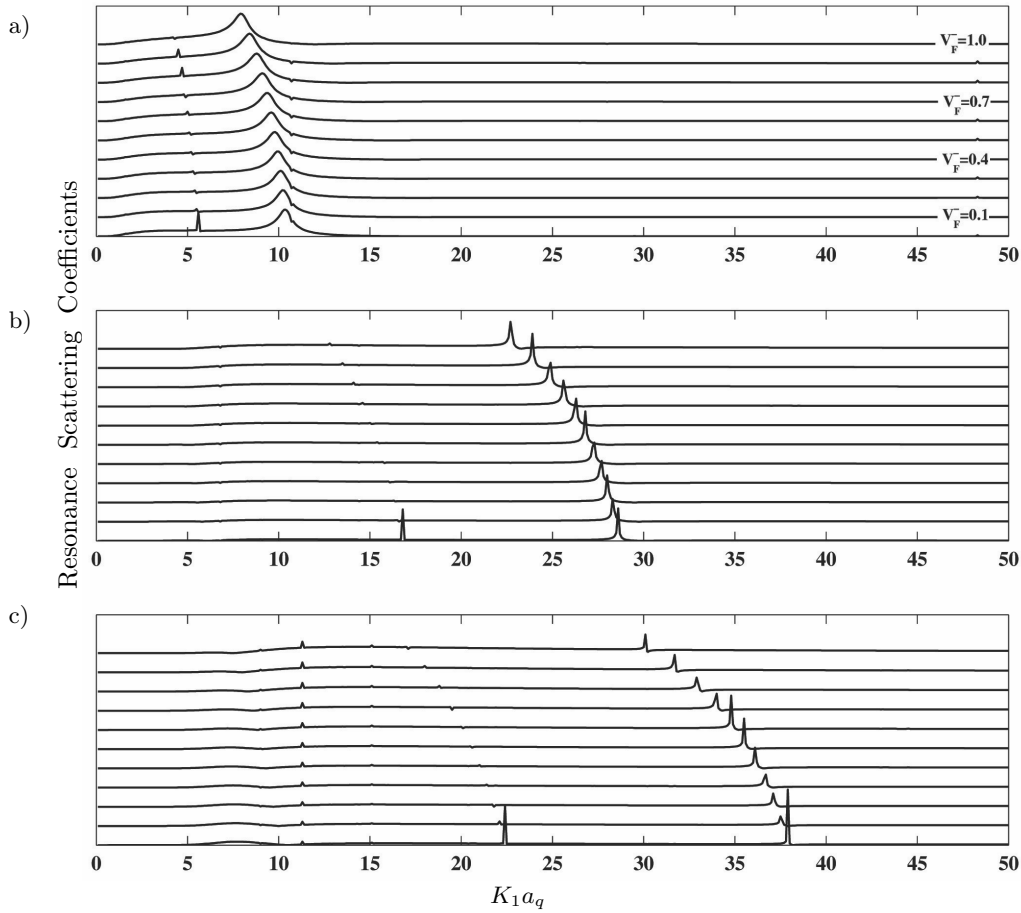


Fig. 8. Variations of the normalized resonance scattering coefficients: a)  $n = 2$ , b)  $n = 6$ , c)  $n = 8$ , with dimensionless frequency, for a thin ( $h/a_q = 0.04$ ) functionally graded hollow cylinder, in case of power-law distribution and for selected values of volume fraction concentration of Al.

citation frequencies) exhibit more variations (i.e., sensitivity) to the change of overall volume fractions of constituting materials. This is due to the fact that for higher mode numbers and in higher ranges of frequencies, the position of the resonances of the single Al shell ( $\bar{V}_F = 1$ ) and the single  $\text{ZrO}_2$  shell ( $\bar{V}_F = 0$ ), with the same eigen-frequency label in each mode number, are generally farther away from each other. Comparing the isolated resonances of thick-graded shell in Fig. 6 with those of the thin shell in Fig. 8, it is observed that in the case of a thick shell, there are more crowded regions of resonances in comparison to the thin shell. Also, the resonance frequencies of the thin shell exhibit less sensitivity to the variation of overall volume fraction of constituents compared to those of a thick shell. In this case, we need to use the resonances corresponding

to higher mode numbers. It is noticeable that in practice, the excitation of resonances corresponding to higher modes at high frequencies is a challenging task and somewhere we should confine ourselves to the lower frequency (fundamental) resonances.

Until now, we have studied the simultaneous effects of the overall volume fractions of the constituting materials and the profile of distribution on the resonances corresponding to the excited surface waves in the thick and thin FGM shells. Here, by examining the frequency response of a thick (i.e.,  $h/a_q = 0.9$ ) and a thin (i.e.,  $h/a_q = 0.04$ ) functionally graded cylindrical shells, where a sigmoid distribution governs the variations of their elastic properties, we intend to isolate the effect of the profile of distribution. Actually, by assuming the sigmoid distribution, we will have a graded shell which for different styles of profiles, its overall volume concentrations of ingredients are restricted in a bound (i.e.,  $0.3 \leq \bar{V}_F \leq 0.5$  in the case of thick shell) or are approximately identical (i.e.,  $\bar{V}_F \cong 0.5$  in the case of a thin shell). In the case of a thick shell, the upper extreme value of the overall volume concentration of Al is  $\bar{V}_F = 0.5$  which corresponds to  $\gamma \rightarrow \infty$  and the lower extreme is  $\bar{V}_F = 0.3$ , which is obtained for  $\gamma = 0$ . Similar to the previous examples, by using a root-finder code, the  $\gamma$  constant in Eq. ((3.1)<sub>2</sub>) may be found so that the discrete values corresponding to the overall volume concentration of Al are obtained. For the thick shell, the discrete values of  $\bar{V}_F = [0.3; 0.32; 0.34; 0.36; 0.38; 0.40; 0.42; 0.44; 0.46; 0.48; 0.50]$  are obtained as  $\gamma = [0.0; 0.34; 0.70; 1.01; 1.68; 2.49; 3.76; 6.02; 11.13; 32.98; 10^2]$ . Clearly,  $\gamma = 10^2$  corresponds to a single shell with properties equivalent to the average of Al and  $\text{ZrO}_2$ , and  $\gamma = 0.0$  corresponds to a double shell (i.e., Al: inner layer and  $\text{ZrO}_2$ : outer layer). Figure 9 shows the volume fraction profiles for some of the discrete

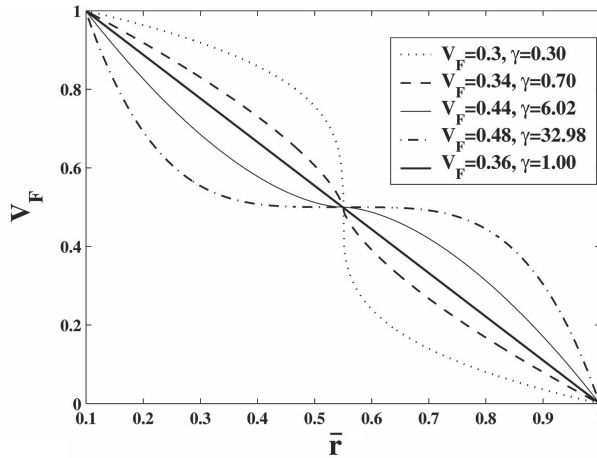


FIG. 9. Variations in volume fraction of aluminum in FGM interlayer of a thick ( $h/a_q = 0.9$ ) functionally graded hollow cylinder in case of sigmoid distribution.

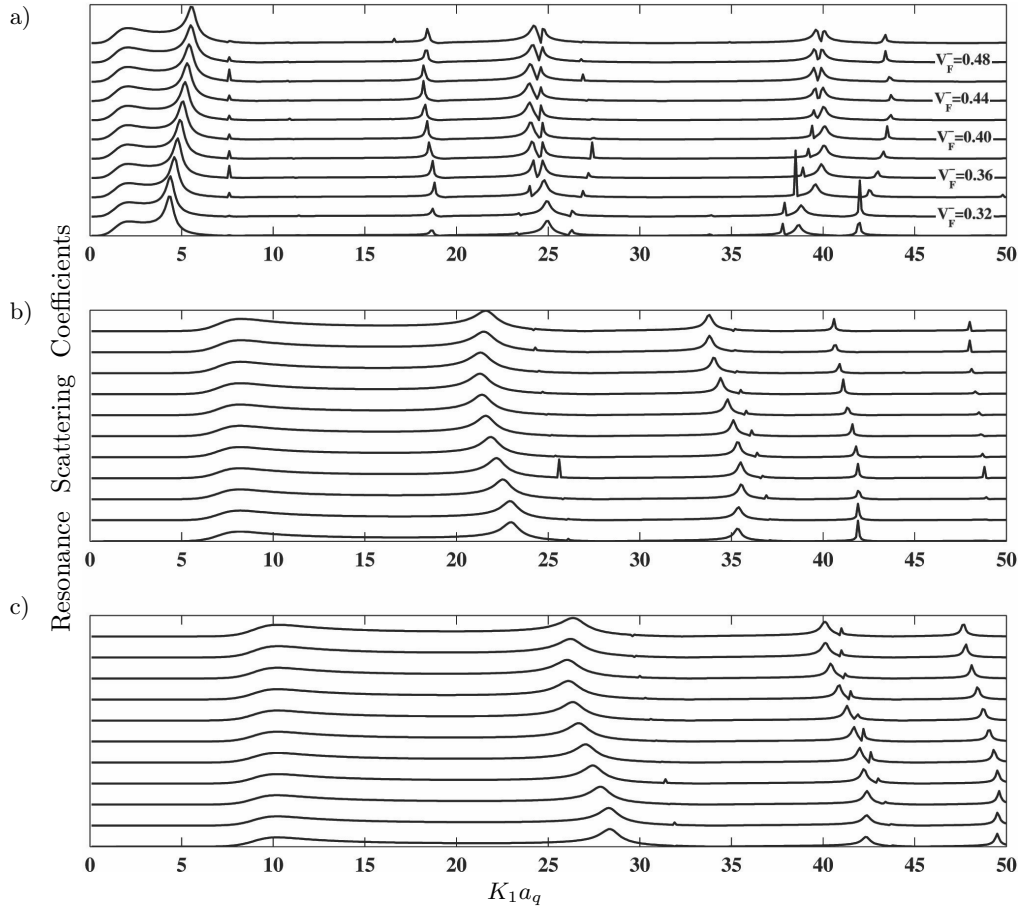


Fig. 10. Variations of the normalized resonance scattering coefficients: a)  $n = 2$ , b)  $n = 8$ , c)  $n = 10$ , with dimensionless frequency, for a thick ( $h/a_q = 0.9$ ) functionally graded hollow cylinder, in case of sigmoid distribution and for selected values of volume fraction concentration of Al.

values of overall volume concentration of Al (i.e.,  $\bar{V}_F = 0.3; 0.34; 0.38; 0.42; 0.46$ ) along the radial axis, for a thick shell. To study the effects of the overall volume concentration of constituting materials and the profile of variations on the resonant response of the graded shell, Figs. 10a–c display the variations of the modal resonance scattering coefficients,  $|f_n^{(\text{res})}(\theta = \pi, K_1 a_q)|$ ; a)  $n = 2$ , b)  $n = 8$ , c)  $n = 10$ . In the case of a thin shell and for a wide range of  $\gamma$ , the volume concentration of Al is approximately constant,  $\bar{V}_F \cong 0.5$ . Therefore, in order to have different profiles, we select  $\gamma = [0.2; 0.5; 1; 2; 5]$ . As Figure 11 shows, the designs corresponding to  $\gamma > 1$  are desirable where a metal-rich composition near the inner interface, and a ceramic-rich composition near the outer interface are

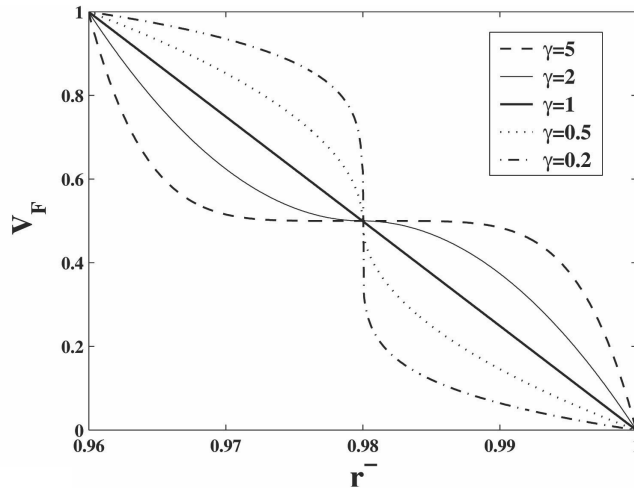


Fig. 11. Variations in volume fraction of aluminum in FGM interlayer of a thin ( $h/a_q = 0.04$ ) functionally graded hollow cylinder, in case of sigmoid distribution.

required. Figures 12a and b display the variations of the modal resonance scattering coefficients,  $|f_n^{(\text{res})}(\theta = \pi, K_1 a_q)|$ , a)  $n = 5$ , b)  $n = 15$ , with dimensionless frequency. The most important observations are as follows. Comparing Fig. 12a with Fig. 6c, which exhibit the resonance scattering coefficients of a  $h/a_q = 0.9$  graded shell, for the same mode number,  $n = 2$ , and for different styles of profiles (i.e., power-law and sigmoid distributions, respectively), indicates that in the case of sigmoid distribution, the variations of the resonance frequencies is evidently less than those of in the case of power-law distribution. Due to the fact that the profiles of distribution are varying in both cases, this observation can be attributed to the restriction on the variations of the overall volume concentrations in the case of the sigmoid distribution. Taking a look at Figs. 10a–c, we observe that several resonance frequencies demonstrate nonlinear and, in some cases, non-monotonic behavior with respect to the linear change of overall volume fractions of constituents. This may be due to the more complex variations of the profiles in the case of sigmoid distribution. Therefore, in the case of intricate profiles, the overall volume concentration of ingredients and the profile of distribution must be evaluated simultaneously and by using a cluster of resonance frequencies. Careful examination of Figs. 10a–c and Figs. 6a–c demonstrate the relatively higher sensitivity of the Rayleigh-type resonances (i.e., first eigenfrequency in each mode number) to the profile of distribution, in comparison with the Whispering Gallery resonances which are excited in higher frequencies. This may be linked to the fact that the displacement field corresponding to this type of surface wave is the result of continuous penetration of elastic waves into the structure and consequently, a better sense of the structure details [37]. More-

over, particular feature corresponding to this type of resonance in Fig. 10a is observed where its frequency of excitation increases with the overall volume fraction of Al.

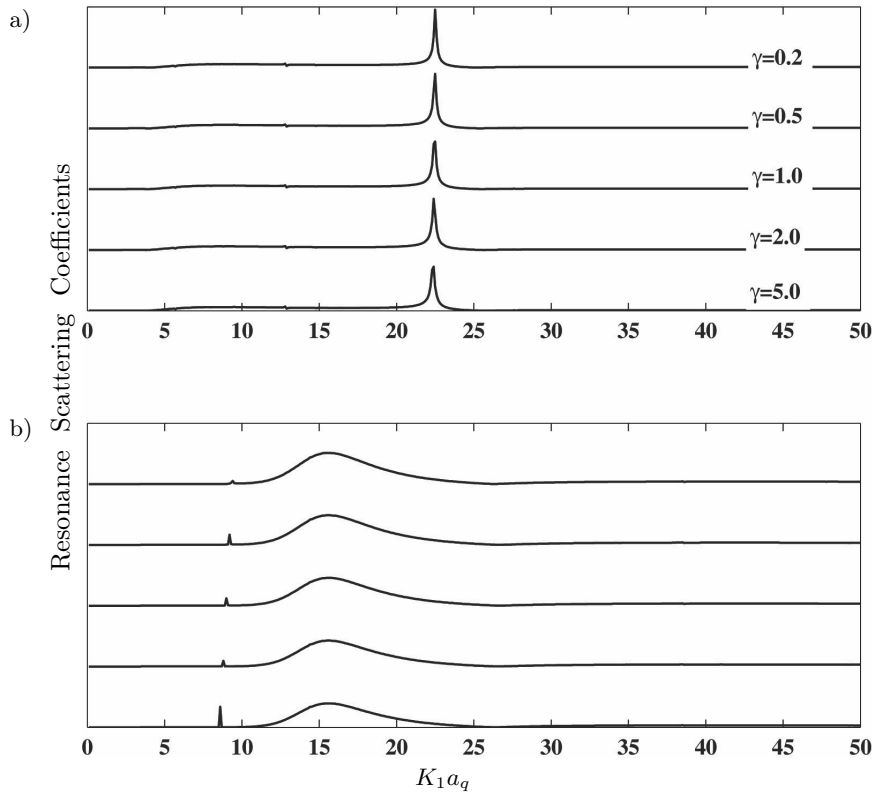


Fig. 12. Variations of the normalized resonance scattering coefficients: a)  $n = 5$ , b)  $n = 15$ , with dimensionless frequency, for a thin ( $h/a_q = 0.04$ ) functionally graded hollow cylinder, in case of sigmoid distribution and for selected values of  $\gamma$ .

As Figure 12 shows, in the selected frequency range,  $0 \leq K_1 a_q \leq 50$ , the back-scattered response of the thin-graded shell for different profiles of variations which have equal volume concentration of ingredients, are the same (even for high mode number,  $n = 15$ ). Comparing these figures with Fig. 8, it is observed that the influence of the overall volume fractions of constituents on the resonance response of the thin-walled graded shells in comparison to the profile of distribution is quite pronounced. This fact may be justified by noting that the excited surface waves in such thin shells are often the zero-order Lamb or the fluid-born A-type waves [37], and the phase velocities associated to these waves are primarily the function of the averaged properties of the shell; therefore, in

their resonance state, the shell vibrates as a whole body such that the least sense of structure's interior is achieved.

### 3.3. Validations

Finally, to check the overall validity of the model, we compute the variations of the global scattering coefficient for an air-filled single-layer aluminum shell submerged in water. For this, we increase the number of layers to  $q = 100$  in the multilayered cylindrical shell by setting  $h/a_q = 0.8$ ,  $q = 100$ ,  $\rho^{(j)} = 2790 \text{ kg/m}^3$ ,  $c_{11}^{(j)} = c_{22}^{(j)} = c_{33}^{(j)} = 113.1 \text{ GPa}$ ,  $c_{44}^{(j)} = c_{55}^{(j)} = c_{66}^{(j)} = 26.7 \text{ GPa}$  where  $j = 1, 2, \dots, 100$ ,  $\rho_1 = 1000 \text{ kg/m}^3$ ,  $c_1 = 1480 \text{ m/s}$ ,  $\rho_2 = 1.2 \text{ kg/m}^3$  and  $c_2 = 344 \text{ m/s}$ . The numerical results, as shown in Fig. 13a, show good agreement with those given in Fig. 1 of [36]. In order to check the FGM models, we compute the variations of the resonance scattering coefficients, for air-filled and water-submerged FGM shells with different thicknesses of FGM interlayer and for different profiles (MR:  $\gamma = 0.2$ , LN:  $\gamma = 0.1$ , CR:  $\gamma = 5.0$ ) by setting  $h/a_q = 0.1$ ,  $q = 100$ ,  $\rho_c^1 = 2790 \text{ kg/m}^3$ ,  $c_{11}^{(1)} = c_{22}^{(1)} = c_{33}^{(1)} = 113.5 \text{ GPa}$ ,  $c_{44}^{(1)} = c_{55}^{(1)} = c_{66}^{(1)} = 26.8 \text{ GPa}$ ,  $c_{12}^{(1)} = c_{13}^{(1)} = c_{23}^{(1)} = 318.0 \text{ GPa}$ ,  $c_{11}^{(q)} = c_{22}^{(q)} = c_{33}^{(q)} = 129.00 \text{ GPa}$ ,  $c_{44}^{(q)} = c_{55}^{(q)} = c_{66}^{(q)} = 94.80 \text{ GPa}$ ,  $\rho_c^{(q)} = 5700 \text{ kg/m}^3$ . For Case I, Case II and Case III, we respectively set  $h_a/h = h_b/h = 0$ ,  $h_a/h = h_b/h = 0.25$  and  $h_a/h = h_b/h = 0.45$ . For all cases, the numerical results, as shown in Fig. 13b, are identical and show good agreement with those shown in Fig. 4 of [26]. At last, in order to check the validity of the described analysis to model the cylindrical anisotropy, we compute the variations of the backscattering form function ampli-

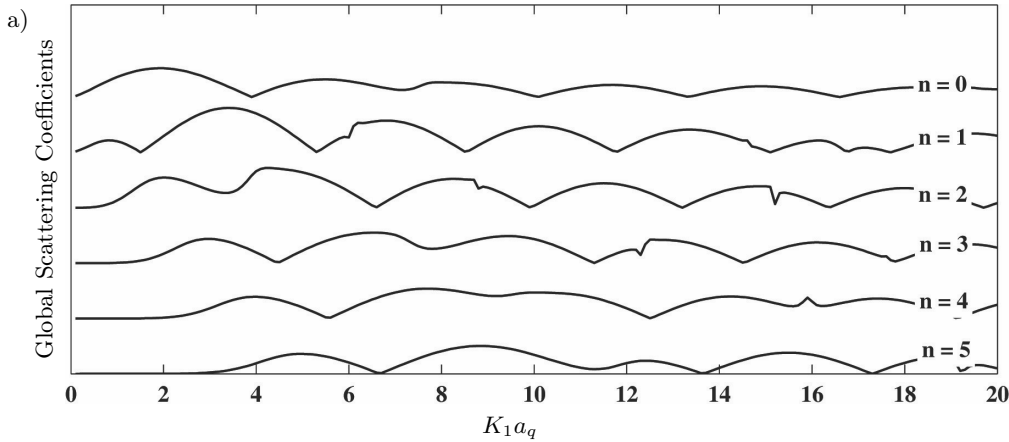


Fig. 13. a) Variations of the modal backscattering form function amplitude with dimensionless frequency for selected mode numbers ( $n = 0, 1, \dots, 5$ ), for an air-filled aluminum shell submerged in water.

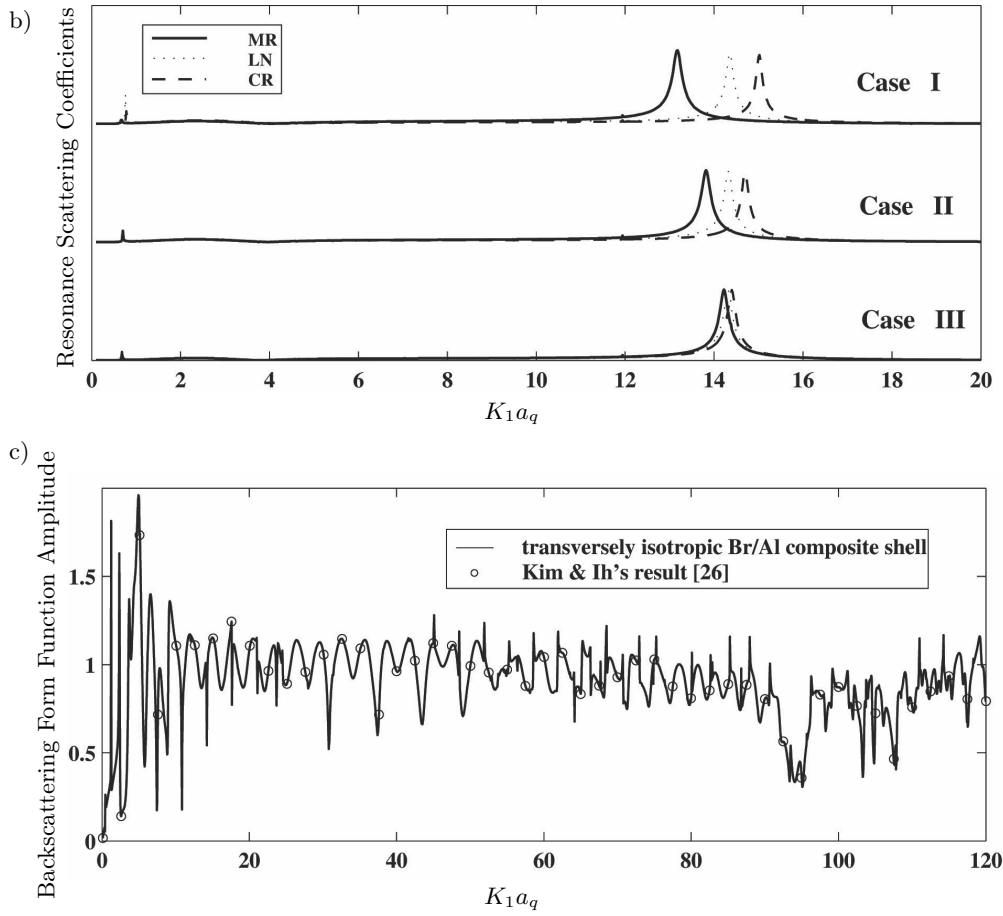


Fig. 13. b) Variations of the resonance scattering coefficient with dimensionless frequency for selected mode number ( $n = 3$ ) for an air-filled and water submerged aluminum shell, moderately thick ( $h/a_q = 0.1$ ) functionally graded hollow cylinder, in case of power-law distribution and for different configurations (Case I:  $h_a/h = h_b/h = 0.0$ , Case II:  $h_a/h = h_b/h = 0.25$ , Case III:  $h_a/h = h_b/h = 0.45$ ) (---  $\gamma = 5$ , .....  $\gamma = 1.00$ , —  $\gamma = 0.2$ ). c) Variations of the backscattering form function with dimensionless frequency, for oblique wave incidence ( $\alpha = 9^\circ$ ), upon an air-filled boron/aluminum unidirectional composite cylindrical shell submerged in water.

tude for oblique incidence ( $\alpha = 9^\circ$ ) upon an air-filled boron/aluminum unidirectional composite cylindrical shell, submerged in water by setting  $h/a_q = 0.16$ ,  $q = 1$ ,  $\rho_c^{(1)} = 2738 \text{ kg/m}^3$ ,  $c_{11}^{(1)} = c_{22}^{(1)} = 142.1 \text{ GPa}$ ,  $c_{12}^{(1)} = 71.1 \text{ GPa}$ ,  $c_{13}^{(1)} = c_{23}^{(1)} = 66.4 \text{ GPa}$ ,  $c_{33}^{(1)} = 219.4 \text{ GPa}$ ,  $c_{44}^{(1)} = c_{55}^{(1)} = 37.1 \text{ GPa}$ ,  $c_{66}^{(1)} = 35.5 \text{ GPa}$ ,  $\rho_1 = 1000 \text{ kg/m}^3$ ,  $c_1 = 1480 \text{ m/s}$ ,  $\rho_2 = 1.2 \text{ kg/m}^3$  and  $c_2 = 340 \text{ m/s}$  in our general MATLAB code. The numerical results, as shown in Fig. 13c, show good agreement with those shown in Fig. 7a in [38].

#### 4. Conclusion

The present work is concerned with acoustic wave scattering from a thick-walled sandwich cylindrical shell with FGM core. For generality of the solution, the cylindrical shell is assumed to be orthotropic and the angle of incidence set to be non-zero. An approximate laminate model, in the context of the so-called state space formulation along with the classical T-matrix solution technique involving a system global transfer matrix as the product of the individual transfer matrices, is employed to solve for the unknown modal scattering and transmission coefficients. Three models, representing the elastic properties of FGM interlayer are considered. In the first two models, the rule of mixture governs. In the third model, an elegant self-consistent micromechanical model which assumes an interconnected skeletal microstructure in the graded region is employed. Examining the back-scattered acoustic response of these models reveals the lower overall stiffness associated to the composite (third) model and consequently, the lower resonance frequencies. In our frequency range, the maximum relative errors may reach to 15 percent which in the case of improper recognition of the model may lead to an extraordinary inaccuracy in NDE process.

The main aim of this work is concerned to investigate the sensitivity of the resonance frequencies of the graded shells to the overall volume fraction of the constituting materials for practical profiles of distribution (i.e., power-law and sigmoidal), in order to make technical points for the resonance acoustic spectroscopy purposes of this kind of composite structures. The results reveal the pronounced effect of the overall volume fraction of constituents on the resonance frequencies of the graded shells, especially in the case of thick shells where the Rayleigh and Whispering Gallery type waves are anticipated. The linear and monotonic correlation between the resonance frequency variations and the overall volume fraction of ingredients may essentially be used for non-destructive evaluation purposes. In addition, comparing the resonant responses corresponding to the power-law and the sigmoid distributions for the same thicknesses of the graded shell, indicates that the changes in the profile of distribution demonstrates itself as higher-order terms in the variations of the resonance frequencies, and the resonance frequencies are primarily affected by the overall volume concentration of constituents rather than the detailed design of the variation's profile. Hence, a number of resonance frequencies must be tracked to estimate the profile of distribution. In the case of thin-walled shells, where the zero-order Lamb-type waves are anticipated, the resonance frequencies exhibit less sensitivity to the distribution's profile in comparison to the Rayleigh and Whispering Gallery waves, especially in the case of sigmoidal distribution. This observation is due to this fact that this type of surface waves is primarily affected by the average bulk properties of the shell rather than the details of the struc-

ture. Evidently, higher resonance frequencies (i.e., lower wavelengths) may be functional assets for interrogating purposes of distribution profiles of graded shells.

## Appendix I

$$\mathbf{M}^k = \begin{bmatrix} \mathbf{M}_{11}^k & \mathbf{M}_{12}^k \\ \mathbf{M}_{21}^k & \mathbf{M}_{22}^k \end{bmatrix},$$

where

$$\begin{aligned} \mathbf{M}_{11}^k &= \begin{bmatrix} \frac{1}{r} & -\frac{\partial}{r\partial\theta} \\ \frac{c_{12}^k}{c_{11}^k} \frac{\partial}{r\partial\theta} & -\frac{c_{12}^k}{c_{11}^k} \frac{1}{r} \end{bmatrix}, & \mathbf{M}_{12}^k &= \begin{bmatrix} 0 & \frac{1}{c_{33}^k} \\ \frac{1}{c_{11}^k} & 0 \end{bmatrix}, \\ \mathbf{M}_{21}^k &= \begin{bmatrix} -\frac{e^k}{r^2} \frac{\partial}{\partial\theta} & \left( \rho_c^k \frac{\partial^2}{\partial t^2} + \frac{e^k}{r^2} \right) \\ \left( \rho_c^k \frac{\partial^2}{\partial t^2} - c_{44}^k \frac{\partial^2}{\partial z^2} - \frac{e^k}{r^2} \frac{\partial^2}{\partial\theta^2} \right) & -\frac{e^k}{r^2} \frac{\partial}{\partial\theta} \end{bmatrix}, \\ \mathbf{M}_{22}^k &= \begin{bmatrix} \frac{1}{r} \left( \frac{c_{12}^k}{c_{11}^k} - 1 \right) & -\frac{\partial}{r\partial\theta} \\ -\frac{c_{12}^k}{c_{11}^k} \frac{\partial}{r\partial\theta} & -\frac{2}{r} \end{bmatrix}, \end{aligned}$$

in which  $e^k = c_{22}^k - \frac{(c_{12}^k)^2}{c_{11}^k}$ .

## Appendix II

$$\mathbf{D}_n^k = \begin{bmatrix} \mathbf{D}_{11,n}^k & \mathbf{D}_{12,n}^k \\ \mathbf{D}_{21,n}^k & \mathbf{D}_{22,n}^k \end{bmatrix},$$

where

$$\mathbf{D}_{11}^k = \begin{bmatrix} \frac{1}{\xi} & \frac{n}{\xi} \\ \frac{c_{12}^k}{c_{11}^k} \frac{n}{\xi} & -\frac{c_{12}^k}{c_{11}^k} \frac{1}{\xi} \end{bmatrix}, \quad \mathbf{D}_{12}^k = \begin{bmatrix} 0 & 1 \\ \frac{c_{33}^k}{c_{11}^k} & 0 \end{bmatrix},$$

$$\mathbf{D}_{21}^k = \begin{bmatrix} -\frac{e^k}{c_{33}^k} \frac{n}{\xi^2} & \frac{1}{c_{33}^k} \left( -\rho_c^k \omega^2 a_q^2 + \frac{e^k}{\xi^2} \right) \\ \frac{1}{c_{33}^k} \left( -\rho_c^k \omega^2 a_q^2 + \frac{e^k n^2}{\xi^2} \right) & \frac{e^k}{c_{33}^k} \frac{n}{\xi^2} \end{bmatrix},$$

$$\mathbf{D}_{22}^k = \begin{bmatrix} \frac{1}{\xi} \left( \frac{c_{12}^k}{c_{11}^k} - 1 \right) & -\frac{n}{\xi} \\ \frac{c_{12}^k}{c_{11}^k} \frac{n}{\xi} & -\frac{2}{\xi} \end{bmatrix}.$$

## References

1. M. YAMANOUCHI, M. KOIZUMI, T. HIRAI, I. SHIOTA, *Proceedings of the First International Symposium on Functionally Gradient Materials*, Sendai, Japan, 1990.
2. J.B. HOLT, M. KOIZUMI, T. HIRAI, Z.A. MUNIR, *Ceramic Transaction: Functionally Gradient Materials*, Vol. 34, The American Ceramic Society, Ohio, Westerville, 1993.
3. M. KOIZUMI, *The concept of FGM*, [in:] *Ceramic Transaction: Functionally Gradient Materials*, J.B. HOLT, M. KOIZUMI, T. HIRAI, Z.A. MUNIR [Eds.], Vol. 34, The American Ceramic Society, Ohio, Westerville, 3–10, 1993.
4. S. SURESH, A. MORTENSEN, *Fundamentals of Functionally Graded Materials*, IOM Communications, London 1998.
5. Y. MIYAMOTO, W.A. KAYSSER, B.H. RABIN, A. KAWASAKI, R.G. FORD, *Functionally Graded Materials: Design, Processing and Applications*, Chapman Hall, 1999.
6. M. TALMANT, H. BATARD, *Material characterization and resonant scattering by cylinders*, Proceedings of the IEEE Ultrasonics Symposium, **3**, 1371–1380, 1994.
7. A. MIGLIORI, J.L. SARRAO, *Resonant Ultrasound Spectroscopy: Applications to Physics, Materials Measurements and Nondestructive Evaluation*, Wiley, New York 1997.
8. A. TESEI, W.L.J. FOX, A. MAGUER, A. LOVIK, *Target parameter estimation using resonance scattering analysis applied to air-filled, cylindrical shells in water*, J. Acoust. Soc. Am., **108**, 2891–2910, 2000.
9. D. GUICKING, K. GOERK, H. PEINE, *Recent advances in sonar target classification*, Proceedings of SPIE – International Society for Optical Engineering, **1700**, 2–15, 1992.
10. F. HONARVAR, A.N. SINCLAIR, *Nondestructive evaluation of cylindrical components by resonance acoustic spectroscopy*, Ultrasonics, **36**, 845–854, 1998.
11. G.C. GAUNAURD, *Elastic and acoustic resonance wave scattering*, Applied Mechanical Review, **42**, 143–192, 1989.
12. H. ÜBERALL, *Acoustic Resonance Scattering*, Gordon and Breach Science, Philadelphia 1992.
13. N.D. VEKSLER, *Resonance Acoustic Spectroscopy*, Springer Series on Wave Phenomena, Springer-Verlag, Berlin 1993.

14. G. KADUCHAK, C.M. LOEFFLER, *Sound scattering by a fluid-filled cylindrical shell in water*, J. Acoust. Soc. Am., **97**, 3423–3424, 1995.
15. N.D. VEKSLER, J.L. IZBICKI, *Modal resonances of peripheral waves*, Acta Acustica, **82**, 401–410, 1996.
16. F. HONARVAR, A.N. SINCLAIR, *Acoustic wave scattering from transversely isotropic cylinders*, J. Acoust. Soc. Am., **100**, 57–63, 1996.
17. Y.S. JOO, J.G. IH, M.S. CHOI, *Inherent background coefficients for acoustic resonance scattering from submerged, multilayered, cylindrical structures*, J. Acoust. Soc. Am., **103**, 900–910, 1998.
18. J.M. CONOIR, J.L. IZBICKI, O. LENOIR, *Phase gradient method applied to scattering by an elastic shell*, Ultrasonics, **35**, 157–169, 1997.
19. M.S. CHOI, Y.S. JOO, J.P. LEE, *The inherent background in acoustic wave scattering by a submerged target*, J. Acoust. Soc. Am., **99**, 2594–2603, 1996.
20. M.S. CHOI, Y.S. JOO, *Theory of the background amplitudes in acoustic resonance scattering*, J. Acoust. Soc. Am., **101**, 2083–2087, 1997.
21. Y.S. JOO, J.G. IH, M.S. CHOI, *Inherent background coefficients for acoustic resonance scattering from submerged, multilayered, cylindrical structures*, J. Acoust. Soc. Am., **103**, 900–910, 1998.
22. H. ÜBERALL, *Acoustics of shells*, Acoustical Physics, **47**, 115–139, 2003.
23. J.Y. KIM, J.G. IH, *Scattering of plane acoustic waves by a transversely isotropic cylindrical shell-Application to material characterization*, Applied Acoustics, **64**, 1187–1204, 2003.
24. Y. FAN, F. HONARVAR, A.N. SINCLAIR, M.R. JAFARI, *Circumferential resonance modes of solid elastic cylinders excited by obliquely incident acoustic waves*, J. Acoust. Soc. Am., **113**, 102–113, 2003.
25. S.M. HASHEMINEJAD, M. RAJABI, *Acoustic scattering characteristics of thick-walled orthotropic cylindrical shell at oblique incidence*, Ultrasonics, **47**, 32–48, 2007.
26. S.M. HASHEMINEJAD, M. RAJABI, *Acoustic resonance scattering from a submerged functionally graded cylindrical shell*, Journal of Sound and Vibration, **302**, 208–228, 2007.
27. A.D. PIERCE, *Acoustics; An Introduction to its Physical Principles and Applications*, American Institute of Physics, New York 1991.
28. W.Q. CHEN, Z.G. BIAN, H.J. DING, *Three-dimensional vibration analysis of fluid filled orthotropic FGM cylindrical shells*, International Journal of Mechanical Sciences, **46**, 159–171, 2004.
29. W.Q. CHEN, Z.G. BIAN, C.F. LV, H.J. DING, *3D free vibration analysis of a functionally graded piezoelectric hollow cylinder filled with compressible fluid*, International Journal of Solids and Structures, **41**, 947–964, 2004.
30. J.D. ACHENBACH, *Wave Propagation in Elastic Solids*, North-Holland, New York 1976.
31. M.J.P. MUSGRAVE, *Crystal Acoustics*, Holden-Day Series in Mathematical Physics, 1970.
32. R. HILL, *A self-consistent mechanics of composite materials*, Journal of Mechanics and Physics of Solids, **13**, 213–222, 1965.

33. T. REITER, G.J. DVORAK, V. TVERGAARD, *Micromechanical models for graded composite materials*, Journal of Mechanics and Physics of Solids, **45**, 1281–1302, 1997.
34. Y.S. JOO, J.G. IH, M.S. CHOI, *Inherent background coefficients for acoustic resonance scattering from submerged, multilayered, cylindrical structures*, J. Acoust. Soc. Am., **103**, 900–910, 1998.
35. M.S. CHOI, *Inherent background coefficient of the axisymmetric mode in acoustic resonance scattering from a system of multilayered shells*, Journal of Korean Physics Society, **37**, 519–526, 2000.
36. J.D. MURPHY, E.D. BREITENBACH, H. UBERALL, *Resonance scattering of acoustic waves from cylindrical shells*, J. Acoust. Soc. Amer., **64**, 677–683, 1978.
37. J. DAVID N. CHEEKE, *Fundamental and Application of Ultrasonic Waves*, CRC Series in Pure and Applied Physics, 2002.
38. J.Y. KIM, J.G. IH, *Scattering of plane acoustic waves by a transversely isotropic cylindrical shell. Application to material characterization*, Applied Acoustics, **64**, 1187–1204, 2003.

Received March 31, 2010; revised version October 22, 2010.

---